Preprint, Astrophysical Journal in press Feb. 25, 1999

BAYESIAN PERIODIC SIGNAL DETECTION. II. DISCOVERY OF PERIODIC PHASE MODULATION IN LS I +61°303 RADIO OUTBURSTS

P. C. Gregory
Department of Physics and Astronomy, University of British Columbia, Vancouver, British Columbia, V6T 1Z1, Canada

M. Peracaula and A. R. Taylor
Department of Physics and Astronomy, University of Calgary, Calgary, Alberta, T2N 1N4, Canada

ABSTRACT

A Bayesian analysis of the phase variations of the 26.5 day periodic radio outbursts from the high mass X-ray binary LS I +61°303 demonstrates a clear periodic modulation on a time scale similar to that previously found for the long term modulation of the outburst peak flux density. Combining the outburst phase and flux information we obtain a phase and flux modulation period of 1584^{+14}_{-11} days as well as a more accurate outburst period of 26.4917 ± .0025 days. From the shape of the phase and outburst flux modulation we find that larger outbursts occur at an earlier orbital phase, closer to periastron, probably as a result of variations in the wind from the rapidly rotating Be star primary. The phase modulation also suggests a rather sudden onset to each new cycle of mass loss by the Be star. The next maximum in long term flux modulation is predicted to occur between February, 1999 and March, 2000 (Julian day 2,451,233 to 2,451,633).

Subject headings: Bayesian methods, period detection, LS I +61°303, Gregory-Loredo method, x-ray binary, neutron star, radio star, pulsar

1. INTRODUCTION

The luminous, massive X-ray binary, LS I +61°303 (V615 Cas, GT 0236+610) is particularly interesting because of its strong variable emission from radio to X-ray. It is also the probable counterpart to the γ-ray source, 2CG 135+01 (Gregory and Taylor 1978, Kniffen et al. 1997). At radio wavelengths it exhibits periodic radio outbursts with a period of 26.5 days (Taylor and Gregory 1982, 1984). The X-ray emission (Bignami et al. 1981; Goldoni & Mereghetti 1995;

Taylor et al. 1996; Leahy, Harrison & Yoshida 1997) is weak (10^{34} erg s^{-1} at maximum) and has been observed to vary by a factor of 10 over an one orbital period (Taylor et al. 1996). Recently Paredes et al. (1997) reported an approximately 5 fold 26.7 ± 0.2 day modulation of the 2-10 keV X-ray flux.

The radio outbursts are not stable in phase. Outburst maxima have been seen from phase 0.45 to 0.95, but bright maxima seem to occur near 0.6 (Paredes, Estalella, & Rius 1990). Furthermore the peak fluxes of the outbursts are known to exhibit a long term ≈ 1600 day modulation (Gregory et al. 1989, Martí 1993, Martí and Paredes 1995, Peracaula 1997, Gregory 1999, hereafter Paper I).

In the period 1977 August to 1992 August a total of 14 outbursts were recorded by a variety of groups. Beginning in January 1994 (Ray et al. 1997) detailed monitoring was performed (several times a day) with the National Radio Astronomy Observatory Green Bank Interferometer (GBI). This has yielded high-quality data for an additional 33 outbursts to date. From an analysis of the GBI data, Ray et al. (1997) reported a secular change in the outburst phase indicating either orbital period evolution, or a drift in orbital phase. Based on the first 2 years of the GBI data (28 cycles) they found only weak evidence for the proposed long term periodic outburst peak flux modulation.

A recent Bayesian analysis of over 20 years of LS I +61°303 data (Paper I) clearly demonstrated the existence of a periodic or quasi-periodic outburst peak flux modulation with a period of 1632 days and a 68% credible range from 1599 to 1660 days. In this paper (Paper II) we report a Bayesian analysis of the outburst phase.

In section 2 of this paper we consider four hypotheses to explain the outburst phase variations that are to be tested and discuss the data. In sections 3 to 6 we describe our Bayesian analysis of these hypotheses. The probabilities of the four hypotheses are compared in section 7, leading to the conclusion that the outburst phase is periodically modulated on a time scale similar to that previously found for the outburst peak flux. Section 8 describes a joint analysis of the phase and flux data and presents final results on the common modulation period, the outburst period, and details of the shape of the phase and flux modulation light curves. In section 9 we discuss the implications of this work in terms of a model of the LS I +61°303 binary system. Our final conclusions are presented in section 10.

2. Hypothesis Space and Data

In a Bayesian analysis the first step is to define the hypothesis space of interest. In this problem we are interested in hypotheses concerning a time series with associated Gaussian errors. In the particular case of LS I +61°303 the time series consists of the times and peak flux densities of the radio outbursts together with their uncertainties. The outburst phase, of primary interest in this paper, is simply related to the timing residual which is the difference between the observed

and predicted outburst time for a given outburst period. There are four hypotheses concerning the outburst times which we consider in this problem. They are:

ABBREVIATION	HYPOTHESES
H_1	Outburst times are consistent with a single period P. The timing residuals are assumed to be independent Gaussian random with an unknown sigma.
H_2	Sudden period change from P_A to P_B sometime during the data gap from August 1992 to August 1994 just prior to start of Green Bank monitoring program.
H_3	Outburst times are consistent with a single period P and a period derivative $\dot{P}$.
H_4	Single period P_1 for all outbursts plus a periodic modulation P_2 of the timing residuals of unknown shape.

The first job is to obtain the probability of each of these hypotheses given prior information represented by the symbol, I, and the data, D. The probability of any hypothesis H_i is given by Bayes's theorem.

$$\begin{aligned} p(H_i \mid D, I) &= \frac{p(H_i \mid I)p(D \mid H_i, I)}{\sum_{H_i} p(H_i \mid I)p(D \mid H_i, I)} \\ &= \frac{p(H_i \mid I)p(D \mid H_i, I)}{p(D \mid I)}. \end{aligned} \tag{1}$$

The prior probability of hypothesis H_i, assuming the truth of the information given to the right of the vertical bar, in this case I, is given by $p(H_i \mid I)$. $p(H_i \mid D, I)$ is the posterior probability of H_i given I and D. The term $p(D \mid H_i, I)$ is called the likelihood function, which stands for the probability of obtaining the data D which we did, if H_i is true.

$$D \equiv t_1, t_2, \cdots, t_N, \tag{2}$$

where t_i are the times of the individual data outbursts. Let t_{pi} represent the predicted outburst times assuming H_i is true. Then we can write:

$$t_i = t_{pi} + e_i, \tag{3}$$

where e_i is a noise term representing the uncertainty in t_i. In general e_i consists of the random measurement errors plus any real signal in the data that cannot be explained by the model. In the absence of a detailed knowledge of the noise distribution, other than it has a finite variance, the maximum entropy principle tells us that a Gaussian distribution would be the most conservative choice (i.e. maximally non-committal about the information we don't have). In this paper we assume a Gaussian distribution for e_i with a variance σ^2. We let s_i = the experimenter's estimate of σ_i, prior to fitting the model and examining the model residuals. In the present case the absolute value of σ_i is not well known and so we introduce a parameter called the noise scale parameter, b, to allow for this which we marginalize over a prior range. For a discussion of marginalization and other aspects of Bayesian analysis the reader is referred to Section 2 of Gregory and Loredo (1992b). The meaning of the b is given by,

$$\frac{1}{\sigma_i^2} = \frac{b}{s_i^2}. \tag{4}$$

Marginalizing over b has the desirable effect of treating anything in the data that can't be explained by the model as noise and this leads to the most conservative estimates of model parameters. We can also use Bayes's theorem to compute $p(b \mid D, \mathrm{Model}, I)$. If the most probable estimate of $b \approx 1$, then the model is doing a good job accounting for everything that isn't measurement noise. If $b < 1$ then either the model is not accounting for significant features in the data or the initial noise estimates, s_i, were low.

Given this prior information we can write the $p(D \mid H_i, I)$ as the product of N Gaussians.

$$\begin{aligned} p(D \mid H_i, I) &= \prod_{i=1}^{N} \frac{1}{\sigma_i\sqrt{2\pi}} e^{-\frac{(t_i - t_{pi})^2}{2{\sigma_i}^2}} \\ &= (2\pi b)^{\frac{N}{2}} \prod_{i=1}^{N} \left[(s_i)^{-1} \exp(-b\, \frac{(t_i - t_{pi})^2}{2{s_i}^2}) \right] \\ &= (2\pi b)^{\frac{N}{2}} \exp(-\frac{b^N}{2}\chi^2_W) \prod_{i=1}^{N} (s_i)^{-1} \end{aligned} \tag{5}$$

where,

$$\chi^2_W = \sum_{i=1}^{N} \frac{(t_i - t_{pi})^2}{{s_i}^2} = \sum_{i=1}^{N} \frac{{e_i}^2}{{s_i}^2} \tag{6}$$

All of the hypotheses (models) to be considered have different parameters (e.g. period, phase, shape) which up to now do not appear explicitly in the likelihood term. Let θ represent the set of parameters of H_i. The particular parameters for each hypothesis will be introduced

later. For comparing the probabilities of the four hypotheses we need to compute the global likelihoods $p(D \mid H_i, I)$ obtained by marginalizing over all the parameters of each model. In this analysis we assume that the prior probabilities of all four hypotheses are equal. Thus the posterior probabilities are determined by the global likelihoods. A feature of the Bayesian analysis is that marginalization of the model parameters required to determine the global likelihoods automatically introduces a quantified Occam's razor, penalizing more complicated models for their greater complexity.

$$p(D \mid H_i, I) = \int_{\theta_l}^{\theta_u} d\theta \; p(\theta \mid I) p(D \mid \theta, H_i, I) \tag{7}$$

For several of the hypotheses we will also use Bayes's theorem to evaluate the probability density function of particular model parameters.

The outburst times, flux densities and errors used in this analysis are given in Table 1 of Paper I. The peak outburst for some outbursts was sufficiently weak that it was not possible to derive an outburst time accurately enough to use in the timing residual analysis. This is indicated by blank in the timing residual and error columns. These outbursts were still included if the coverage was sufficient to provide information about the flux density. Similarly in two cases it was only possible to obtain a lower limit on the flux density but it was still possible to obtain useful information on the outburst times. This table contains information on a total of 57 outbursts spanning 7520 days.

3. Model Hypothesis H_1

$H_1 \equiv$"outburst times are consistent with a single period P. The timing residuals are assumed to be independent Gaussian random with an unknown σ". This is the simplest hypothesis in our space of hypotheses. According to H_1 the only reason for a difference between t_i and t_{pi} is because of errors in determining the outburst times. For this model t_{pi} is given by:

$$t_{pi} = t_{p0} + P \; \mathrm{nint}(\frac{t_i - t_{p0}}{P}), \tag{8}$$

where nint $\equiv$ nearest integer value, t_{p0} is the predicted outburst time for some particular outburst chosen as a reference whose observed time is t_0. As with any outburst time, t_0 will have an associated error but because it acts as a reference its error will systematically affect all $(t_i - t_{pi})$ terms. We can allow for an unknown systematic error in this quantity by introducing a reference offset parameter $E0$ and then marginalizing over it, where $E0$ is defined by,

$$E0 = t_0 - t_{p0}. \tag{9}$$

Equation (8) can be rewritten in terms of the measured times and model parameters as,

$$t_{pi} = t_0 - E0 + P \text{ nint}(\frac{t_i - t_0 + E0}{P}), \tag{10}$$

The use of equation (8) assumes that the errors in the outburst times are less than $P/2$ or approximately 13 days. There are two criteria for selecting a reference outburst. It should be a well defined outburst and result in timing residuals for the most probable set of parameter values that are roughly symmetrical distributed about zero.

There is one additional parameter for the H_1 model, b, because the model assumes any timing residuals are Gaussian with an unknown value of $\sigma = s_i \; b^{-0.5}$ which can be larger than the timing uncertainties quoted in Table 1 of Paper I. The global likelihood is given by:

$$\begin{aligned} p(D \mid H_1, I) &= \int_{E0_{LO}}^{E0_{HI}} dE0 \; p(E0 \mid H_1, I) \int_{P_{LO}}^{P_{HI}} dP \; p(P \mid H_1, I) \\ &\times \int_{b_{LO}}^{b_{HI}} db \; p(b \mid H_1, I) p(D \mid E0, P, b, H_1, I), \end{aligned} \tag{11}$$

where the priors for $P,\ E0,\ \&\ b$ are assumed to be independent. Since P and b are scale parameters (always positive) we will use a normalized Jeffreys prior of the form,

$$p(b \mid H_1, I) = \frac{1}{b \ln \frac{b_{HI}}{b_{LO}}}, \tag{12}$$

where $b_{LO} = 0.05$ and $b_{HI} = 1.95$ are the prior upper and lower limits used in this paper.

$$p(P \mid H_1, I) = \frac{1}{P \ln \frac{P_{HI}}{P_{LO}}}. \tag{13}$$

A Jeffreys prior assigns equal probability per decade of the prior parameter range. See section 3.2 of Paper I for the rationale behind the choice of a Jeffreys prior. We set $P_{LO} = 25.0$ and $P_{HI} = 28.0$ days in this analysis.

We will use a normalized uniform prior for the location parameter $E0$, of the form,

$$p(E0 \mid H_1, I) = \frac{1}{\Delta E0}, \tag{14}$$

where $\Delta E0 = E0_{HI} - E0_{LO} = (+5) - (-5) = 10$ days.

The final term that needs to be specified is $p(D \mid E0, P, b, H_1, I)$.

$$p(D \mid E0, P, b, H_1, I) = (2\pi b)^{\frac{N}{2}} \; \exp(-\frac{b^N}{2} \chi^2_W) \prod_{i=1}^{N} (s_i)^{-1}, \tag{15}$$

where χ^2_W is given by equation (6).

Substituting equations (13), (14) and (15) into (11) and rearranging yields,

$$\begin{aligned} p(D \mid H_1, I) &= (2\pi)^{-\frac{N}{2}} \frac{1}{\Delta E0} \frac{1}{\ln \frac{P_{HI}}{P_{LO}}} \frac{1}{\ln \frac{b_{HI}}{b_{LO}}} \prod_{i=1}^{N} (s_i)^{-1} \\ &\times \int_{E0_{LO}}^{E0_{HI}} dE0 \int_{P_{LO}}^{P_{HI}} \frac{dP}{P} \int_{b_{LO}}^{b_{HI}} \frac{db}{b}\, b^{(\frac{N}{2})} \exp(-\frac{b^N}{2}\chi^2_W). \end{aligned} \tag{16}$$

The last integral in equation (16) can be evaluated in terms of the incomplete gamma function $P(a, x)$,

$$P(a, x) = \frac{1}{\Gamma(a)} \int_0^x e^{-t} t^{a-1} dt. \tag{17}$$

$$\int_{b_{LO}}^{b_{HI}} \frac{db}{b}\, b^{(\frac{N}{2})} \exp(-\frac{b^N}{2}\chi^2_W) = (\frac{\chi^2_W}{2})^{-\frac{N}{2}}\ \Gamma(\frac{N}{2}) \left[P(\frac{N}{2}, \tau_{HI}) - P(\frac{N}{2}, \tau_{LO}) \right], \tag{18}$$

where,

$$\tau_{HI} = \frac{b_{HI}\ \chi^2_W}{2} \quad \text{and} \tau_{LO} = \frac{b_{LO}\ \chi^2_W}{2} \tag{19}$$

The reference outburst chosen for H_1 was number 28.

We are also interested in $p(P \mid D, H_1, I)$ and $p(E0 \mid D, H_1, I)$ (equation (20) & (21)), the marginal probability density function of the period and $E0$ for this model. This enabled us to compute the most probable timing residuals $(t_i - t_{pi})$, to look for any systematics effects in the residuals of this model.

$$\begin{aligned} p(P \mid H_1, I) &= (2\pi)^{-\frac{N}{2}} \frac{1}{\Delta E0} \frac{1}{\ln \frac{P_{HI}}{P_{LO}}} \frac{1}{\ln \frac{b_{HI}}{b_{LO}}} \prod_{i=1}^{N} (s_i)^{-1} \\ &\times \int_{E0_{LO}}^{E0_{HI}} dE0 \int_{b_{LO}}^{b_{HI}} \frac{db}{b}\, b^{\frac{N}{2}} \exp(-\frac{b^N}{2}\chi^2_W)\ / p(D \mid H_1, I). \end{aligned} \tag{20}$$

$$\begin{aligned} p(E0 \mid H_1, I) &= (2\pi)^{-\frac{N}{2}} \frac{1}{\Delta E0} \frac{1}{\ln \frac{P_{HI}}{P_{LO}}} \frac{1}{\ln \frac{b_{HI}}{b_{LO}}} \prod_{i=1}^{N} (s_i)^{-1} \\ &\times \int_{P_{LO}}^{P_{HI}} \frac{dP}{P} \int_{b_{LO}}^{b_{HI}} \frac{db}{b}\, b^{\frac{N}{2}} \exp(-\frac{b^N}{2}\chi^2_W). \end{aligned} \tag{21}$$

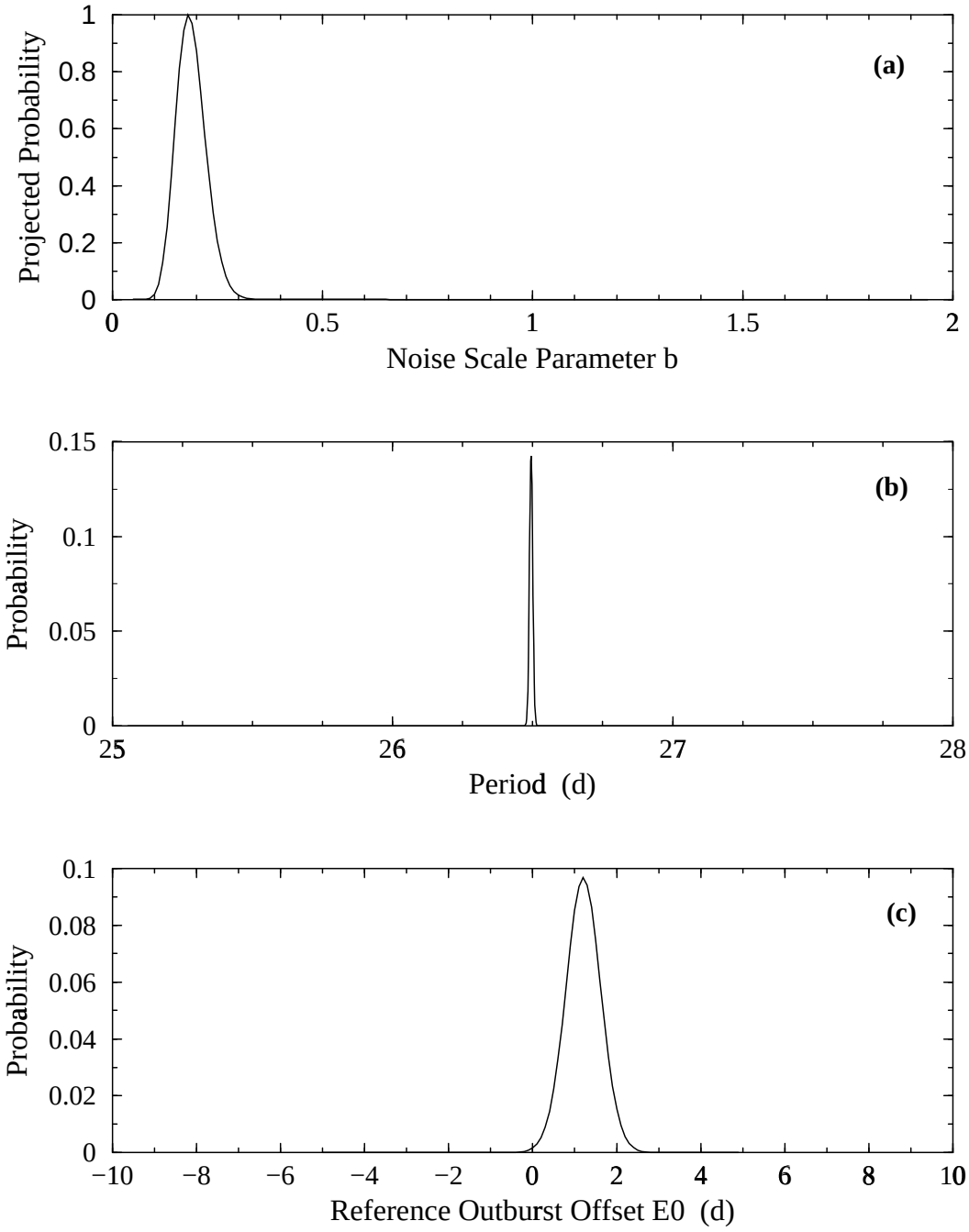

Fig. 1.— Panel (a) shows the projected probability (see text for definition) of the noise scale parameter, b. Panel (b) gives the marginal probability density function for the period from equation (20) and (c) the marginal probability density function of the reference outburst offset, $E0$.

3.1. Results for H_1

We can extract useful information about what the data and our prior information have to say about the noise scale parameter, b, by computing the marginal posterior probability density of b. In figure 1(a) we have plotted what we call the projected probability of b for the prior range of $b = 0.05 \; - \; 1.95$. It is equal to the product of the projection of the multidimensional likelihood, $p(D \mid P, E0, b, H_1, I)$ on to the b axis times our prior for b, $p(b \mid H_1, I)$. In this work we use the projected probability because in practice it is often a reasonable approximation to the marginal and is much easier to compute. The most probable value of $b = 0.18$ means that the effective noise for model H_1, namely everything that can't be fit by this model, is $\approx 1/\sqrt{0.18} = 2.35$ times the estimated noise sigma.

Figure 1(b) shows the marginal probability density function of the period computed from equation (20) based on all the outburst times. The most probable period is $P = 26.494$ days with a 68.3 % ("1 sigma") credible region (CR) extending from 26.488 to 26.499 days.

Figure 1(c) shows the marginal probability density function of the reference offset, $E0$, computed from equation (21). The most probable offset is $E0 = 1.1$ days with a 68.3 % CR extending from 0.7 to 1.5 days.

Figure 2 shows the most probable timing residuals for hypothesis H_1 computed from equation (22) using the most probable values of P and $E0$. The time axis is in days measured from the first peak of the first outburst on Julian day 2443382.94.

$$\text{resid}_i = t_i - t_0 + E0 - P \; \text{nint}(\frac{t_i - t_0 + E0}{P}). \tag{22}$$

The global likelihood of this model, $p(D \mid H_1, I)$ computed from equation (16) is compared to the global likelihood of H_2, H_3 and H_4 in section 7. Although it was the least probable hypothesis it was an important first step in deciding what other models to consider. Examination of the residuals in figure 2 clearly show a systematic trend especially for the GBI outburst times starting around a time of approximately 6000 days which was first noted by Ray et al. (1997). The RMS outburst timing residuals for H_1 are 2.80 days.

4. Model Hypothesis H_2

The results presented by Ray et al. (1997) suggested a period significantly different from our earlier period estimates based on the pre-GBI data. We therefore decided to explore the possibility of hypothesis $H_2 \equiv$ "a sudden period change from P_A to P_B sometime during the 485 day data gap, just prior to the start of GBI monitoring program".

As before D stands for the proposition representing the entire data set of outburst times. We now write $D \equiv D_1, D_2$, the logical conjunction of propositions D_1 and D_2, where D_1 represents

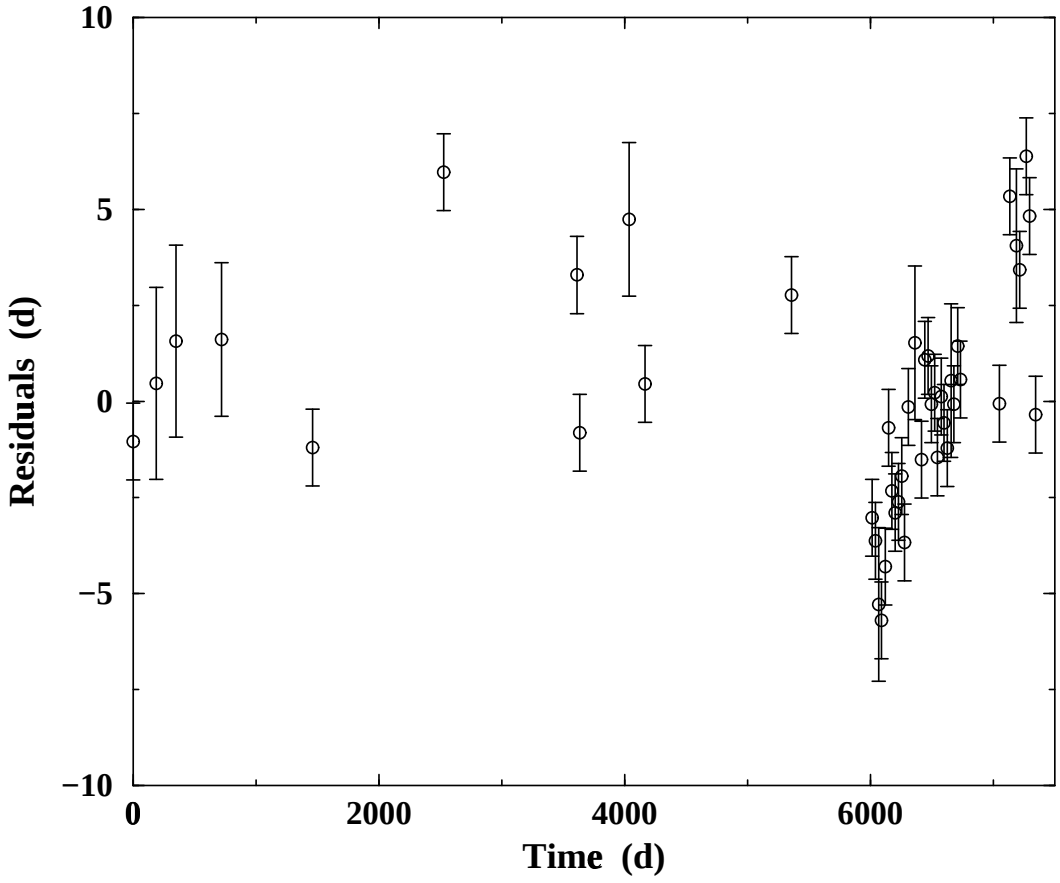

Fig. 2.— The timing residuals assuming a single period for all of the data, hypothesis H_1.

the pre-GBI data (prior to Julian Day 2,449,000.0) with 12 well determined outburst times, and D_2 the GBI data with 33 well determined outburst times. Applying Bayes's theorem we can now compute $p(H_2 \mid D, I)$.

The global likelihood $p(D \mid H_2, I)$ is given by:

$$p(D \mid H_2, I) = p(D_1, D_2 \mid H_2, I) = p(D_1 \mid H_2, I)p(D_2 \mid H_2, I), \tag{23}$$

where we assume D_1 and D_2 are independent.

The equations for $p(D_1 \mid H_2, I)$ and $p(D_2 \mid H_2, I)$ have exactly the same form as equation (16) with N, P, EO, b, χ^2_W replaced by $N_j, P_j, E0_j, b_j, \chi^2_{Wj}$ where $j = 1$ or 2 corresponding to data sets D_1 and D_2 respectively. Also equations for $p(P_j \mid D_j, H_2, I)$ and $p(E0_j \mid D_j, H_2, I)$ have the same form as equations (20) and (21), respectively. For D_1 and D_2 the reference outbursts chosen were 5 and 16, respectively, according to Table 1 in Paper I.

4.1. Results for H_2

The global likelihood of this model, $p(D \mid H_2, I)$ computed from equation (23) is compared to the global likelihood of H_1, H_3 and H_4 in section 7. Keep in mind that our Bayesian calculation automatically includes a quantitative Occam's razor penalizing H_2 for its extra complexity. The most probable values of b for the two data sets were $b = 0.24$ for pre-GBI data and $b = 0.55$ for GBI data. Examination of the RMS timing residuals for H_2 show that they have dramatically decreased for the GBI portion of the data to 1.6 days, while the pre-GBI data RMS residuals are 2.3 days. These need to be compared to the H_1 residuals of 2.8 days.

Figure 3 shows the marginal probability density function for the two periods on the same plot. The most probable $P_A = 26.509$ days with a 68.3 % credible region extending from 26.498 to 26.520 days. The most probable $P_B = 26.649$ days with a 68.3 % CR extending from 26.632 to 26.661 days. The results for $E0$ were $E0_1 = -1.00$ days (68.3 % CR = -2.4, 0.4 days) and for $EO_2 = 0.80$ days (68.3 % CR = 0.55, 1.00 days).

5. Model Hypothesis H_3

In this section we consider the question of whether the measured timing residuals could be accounted for by a period derivative. $H_3 \equiv$"outburst times are consistent with a single period P and period derivative $\dot{P}$". It is more convenient to work in terms of $f = P^{-1}$ and $\dot{f} = -P^{-2}\dot{P}$, where $f = f_0 + \dot{f}(t_i - t_{p0})$. For this model t_{pi} is given by the solution to,

$$f_0(t_{pi} - t_{p0}) + 0.5\dot{f}(t_{pi} - t_{p0})^2 = N_{cycle}, \tag{24}$$

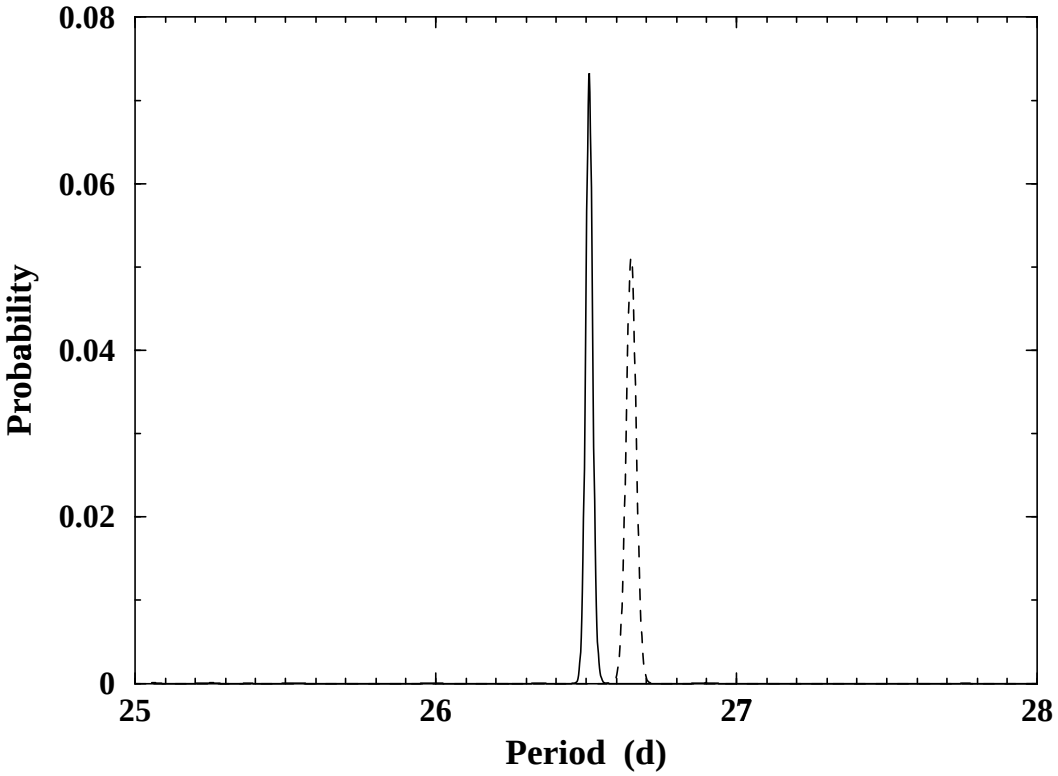

Fig. 3.— The marginal probability density function of the periods, P_1 (solid) and P_2 (dashed) for the two data sets D_1 and D_2, respectively.

where again $t_{p0} = t_0 - E0$ and N_{cycle} is given by,

$$N_{cycle} = \mathrm{nint}(f_0(t_i - t_{p0}) + 0.5\dot{f}(t_i - t_{p0})^2). \tag{25}$$

The physically meaningful solution to the equation (24) is,

$$t_{pi} = t_0 - E0 + \frac{\sqrt{({f_0}^2 + 2N_{cycle}\dot{f})}}{\dot{f}}. \tag{26}$$

When $\dot{f} = 0$ equation (26) breaks down and we need to use equation (8). In this model we have 4 parameters $f, \dot{f}, E0, b$ or equivalently $P, \dot{P}, E0, b$. Again we assume independent parameter priors and use the same priors for $E0$ and b as in section 3. Like P, frequency f is a scale parameter so we will use a Jeffreys prior. The frequency derivative can have either sign so we will use a uniform prior for $\dot{f}$. Therefore we write,

$$p(f \mid H_3, I) = \frac{1}{f \ln \frac{f_{HI}}{f_{LO}}}. \tag{27}$$

and,

$$p(\dot{f} \mid H_3, I) = \frac{1}{\Delta\dot{f}}, \tag{28}$$

where $\Delta\dot{f} = \dot{f}_{HI} - \dot{f}_{LO} = (3.0 \times 10^{-7}) - (-3.0 \times 10^{-7}) = 6.0 \times 10^{-7}\ d^{-2}$. We use a prior range for f corresponding to the P_{HI} and P_{LO} used in section 3.

Following equation (16) the global likelihood for H_3 is given by,

$$\begin{aligned} p(D \mid H_3, I) &= (2\pi)^{-\frac{N}{2}} \frac{1}{\Delta E0} \frac{1}{\Delta\dot{f}} \frac{1}{\ln \frac{f_{HI}}{f_{LO}}} \frac{1}{\ln \frac{b_{HI}}{b_{LO}}} \prod_{i=1}^{N} (s_i)^{-1} \int_{\dot{f}_{LO}}^{\dot{f}_{HI}} d\dot{f} \\ &\times \int_{f_{LO}}^{f_{HI}} \frac{df}{f} \int_{E0_{LO}}^{E0_{HI}} dE0 \int_{b_{LO}}^{b_{HI}} \frac{db}{b}\, b^{(\frac{N}{2})} \exp(-\frac{b^N}{2}\chi^2_W). \end{aligned} \tag{29}$$

where χ^2_W is given by equation (6). Again the last integral in equation (29) can be evaluated in terms of the incomplete gamma function $P(a, x)$ according to equations (17), (18), and(19). The reference outburst chosen for H_3 was number 28.

We can also compute $p(f \mid D, H_3, I)$, $p(\dot{f} \mid D, H_3, I)$ and $p(E0 \mid D, H_3, I)$ in a similar fashion to equations (20) and (21) for $p(P \mid D, H_3, I)$ and $p(E0 \mid D, H_3, I)$ in section 3.

5.1. Results for H_3

The most probable value of $b = 0.25$ means that the effective noise for model H_3, namely everything that can't be fit by this model, is $\approx 1/\sqrt{0.25} = 2.0$ times the estimated noise sigma. Figures 4(a) and (b) show the marginals for P and $\dot{f}$, where, $\dot{P}$ is related to the computed $\dot{f}$ by

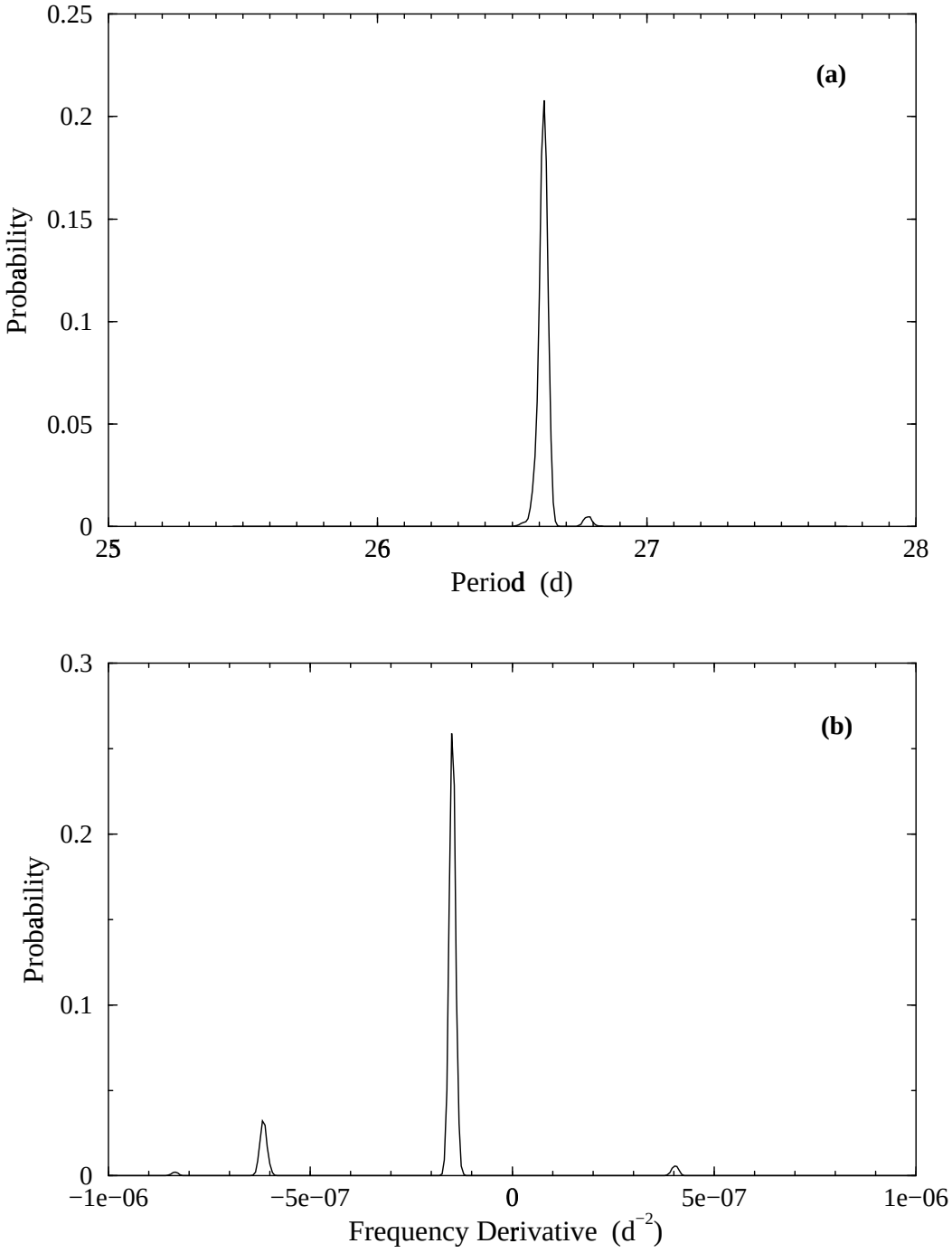

Fig. 4.— The marginal probability density function for the period is shown in (a) and the frequency derivative in (b).

$\dot{P} = -P^2\ \dot{f}$ assuming the most probable value of P. The most probable period is $P = 26.618$ days with a 68.3 % ("1 sigma") credible region (CR) extending from 26.607 to 26.628 days. The most probable period $\dot{P} = 1.04 \times 10^{-4}$ d/d with a credible region (CR) extending from 0.98×10^{-4} to 1.11×10^{-4} d/d. The most probable offset is $E0 = 2.2$ days. It's not surprising that with an extra degree of freedom H_3 is able to explain more of the timing residuals than H_1, however, the derived value of $\dot{P}$ is very large and difficult to account for.

The global likelihood of this model, $p(D \mid H_3, I)$ computed from equation (29) is compared to the global likelihood of the other models in section 7.

6. Model Hypothesis H_4

Recall hypothesis H_4 stands single period P_1 for all outbursts plus a periodic modulation P_2 of the timing residuals of unknown shape. This hypothesis was considered in spite of the fact that a cursory examination of the timing residuals for H_1 (figure 2) failed to indicate any obvious periodicity. The two arguments in support of such a study were: (a) evidence of a long term modulation ($\approx$ 1600 day period) of the flux density of the outbursts, first proposed by Gregory et al. (1989) and recently confirmed by Paper I, and (b) the availability of a Bayesian method for detecting periodicities of unknown shape in nonuniformily sampled time series (Gregory and Loredo 1992a, b, 1993; henceforth referred to as GL1, GL2 and GL3). For an example of its use in X-ray astronomy see Gregory and Loredo (1996). Paper I extended the theory of the GL method to deal with the Gaussian noise case of interest here. Within the range of the search parameter space the GL method identifies the most organized periodic structure, i.e. the structure having the least entropy.

In Paper I we used the GL method to analyze the peak outburst flux densities. The data consisted of the measured peak outburst times and fluxes. In this case the two quantities are the outburst time and timing residual which depends on the assumed outburst period. The outburst period P_1 is believed to correspond to the orbital period which is not accurately known independent of the radio data. For this analysis we treat P_1 as unknown parameter as well. Thus the parameter space being searched for evidence of a periodic structure in the timing residuals is larger than that considered in the flux modulation problem because of the additional period.

In this analysis we will rewrite the outburst times as,

$$t_i = t_{pi} + \tau_i, \tag{30}$$

where,

$$t_{pi} \equiv \text{"predicted outburst times for a given choice of } P_1\ \text{"}, \tag{31}$$

and,

$$\tau_i \equiv \text{"outburst timing residuals "}, \tag{32}$$

where,

$$\tau_i = \tau_{pi} + e_i, \tag{33}$$

where,

$$\tau_{pi} \equiv \text{“predicted outburst timing residuals ”}. \tag{34}$$

Now define the propositions $D_1 \equiv \{t_{pi}\}$ and $D_R \equiv \{\tau_i\}$. Then $D \equiv \{t_i\}$ is the logical conjunction of D_1 and D_R which can be written as the logical statement,

$$D = D_1, D_R \tag{35}$$

As before to determine the probability of H_4 we need to compute the likelihood function $p(D \mid H_4, I)$. Let θ stand for set of parameters required by H_4, which includes P_1. We have not included $E0$, the reference outburst timing offset because we are looking for a periodic pattern in the timing residuals and a small DC offset has no effect on this calculation. In addition θ includes other parameters associated with the modulation periodicity which will be introduced shortly. The likelihood can be rewritten as,

$$\begin{aligned} p(D \mid H_4, I) &= \int d\theta \; p(D, \theta \mid H_4, I) \\ &= \int d\theta \; p(D_1, D_R, \theta \mid H_4, I). \end{aligned} \tag{36}$$

But by the product rule,

$$p(D_1, D_R, \theta \mid H_4, I) = p(D_R, \theta \mid H_4, I) \; p(D_1 \mid D_R, \theta, H_4, I). \tag{37}$$

Since D_1 is deterministically determined from D by the choice of P_1, one of the θ parameters, then

$$p(D_1 \mid D_R, \theta, H_4, I) = 1, \tag{38}$$

and therefore,

$$p(D \mid H_4, I) = \int d\theta \; p(D_R, \theta \mid H_4, I) \tag{39}$$

We now turn to a consideration of the full complement of θ parameters and on how to proceed with the evaluation of equation (39).

6.1. Evaluation of the Likelihood $p(D \mid H_4, I)$

The GL method employs a stepwise (histogram) class of models which is capable of describing any arbitrary periodic light curve with an accuracy determined by the histogram bin size. Since

for an unknown light curve the number of bins, m, required is not known, m is treated as a parameter. Each particular choice of m corresponds to one member, M_m, of the class of periodic models represented by H_4. The Bayesian posterior probability for a periodic model contains a term which quantifies Occam's razor, penalizing successively more complicated periodic models (increasing m) for their greater complexity even though they are assigned equal prior probabilities. The calculation balances model simplicity with goodness-of-fit.

Each periodic model has $m+4$ parameters: the outburst period, P_1, the modulation period, P_2, the phase, ϕ, between the start of the first bin and the start of the data, the noise scale parameter, b, and m shape parameters represented by a vector $\vec{r}$, where r_i specifies the height of the light curve for the i^{th} bin. A remarkable feature of the stepwise model is that it enables marginalization of the m shape parameters to be performed analytically, leaving only the two periods, phase, and noise scale parameter to be marginalized numerically.

The global likelihood for M_m can be obtained from equation (27) of Paper I) after allowing for the additional parameter P_1 and is given by equation (41) below. Note the periods have been expressed as angular frequencies, ω_1 and ω_2 to be consistent with the terminology of Paper I where $\omega = 2\pi/P$. The prior range for the radio outburst period used in this analysis was $P_1 = 25.0$ to 28.0 d, the same as for the other hypotheses. Since the ω_1 is a scale parameter we have used a Jeffreys prior of the form,

$$p(\omega_1 \mid H_4, I) = \frac{1}{\omega_1 \; ln\frac{\omega_{1_{HI}}}{\omega_{1_{LO}}}}. \tag{40}$$

Since the prior range of ω_1 is much less than one decade, a uniform prior for ω would have done just as well. The prior range assumed for the modulation period was $P_2 = 800$ to 2508 d, as in Paper I. The global likelihood for M_m is given by

$$\begin{aligned} p(D \mid M_m, I) &= \frac{(2\pi)^{-\frac{N}{2}}(\Delta r)^{-m}\{\prod_{i=1}^{N}(s_i)^{-1}\}(\frac{\pi}{2})^{m/2}}{2\pi \;\; \ln\frac{\omega_{1_{HI}}}{\omega_{1_{LO}}} \;\; \ln\frac{\omega_{2_{HI}}}{\omega_{2_{LO}}} \ln\frac{b_{HI}}{b_{LO}}} \int \frac{d\omega_1}{\omega_1} \int \frac{d\omega_2}{\omega_2} \int d\phi \int \frac{db}{b} \; b^{\frac{N-m}{2}} \\ &\times \;\; \exp(-\frac{b}{2}\sum_{j=1}^{m}\chi^2_{Wj}) \prod_{j=1}^{m}\{{W_j}^{-1/2}\,[\mathrm{erfc}(y_{jmin}) - \mathrm{erfc}(y_{jmax})\;]\}. \end{aligned} \tag{41}$$

The meaning of the various terms in this analysis are as follows:

$$\chi^2_{Wj} = \sum_{i=1}^{n_j} \frac{(\tau_i - \overline{\tau_{Wj}})^2}{{s_i}^2}, \tag{42}$$

where τ_i is the timing residual of the i^{th} outburst that falls in j^{th} bin of the M_m stepwise model of the P_2 period, N is the total number of outburst times and n_j is the number of outburst times which fall in bin j for a given choice of ω_2 and phase, ϕ. The value of the subscript j corresponding to any particular sample time t is given by,

$$j(t) = \mathrm{int}[1 + m\{(\omega_2 t + \phi) \bmod 2\pi\}/2\pi], \tag{43}$$

where int $\equiv$ integer part of the expression.

We compute the timing residuals from $\tau_i = t_i - t_{pi}$ with t_{pi} given by,

$$t_{pi} = t_0 + P_1 \text{ nint}(\frac{t_i - t_0}{P_1}), \tag{44}$$

and t_0 is the observed time of the reference outburst number 28 (Julian Day 2,449,850.01). The remaining terms in equation (41) are:

$$W_j = \sum_{i=1}^{n_j} \frac{1}{{s_i}^2}, \tag{45}$$

$$y_{jmin} = \sqrt{\frac{bW_j}{2}}(r_{min} - \overline{\tau_{W_j}}) \quad ; \quad y_{jmax} = \sqrt{\frac{bW_j}{2}}(r_{max} - \overline{\tau_{W_j}}), \tag{46}$$

where,

$$\overline{\tau_{Wj}} = \frac{\sum_{i=1}^{n_j} \frac{\tau_i}{s_i^2}}{W_j}, \tag{47}$$

and $r_{min} = -15,\ r_{max} = 15$ days are the prior lower and upper limits on the unknown periodic timing residual modulation used in his analysis. $\Delta r = r_{max} - r_{min}$.

Finally to compute the global likelihood for H_4 we simply sum the likelihoods for each M_m periodic model which were assumed to have equal prior probability.

6.2. Estimating the Periods, P_1 and P_2

The posterior probability of P_2, the period of the outburst timing residual modulation, follows from equations (38) and (39) of Paper I.

$$\begin{aligned} p(\omega_2 \mid D, M_m, I) &= \frac{C}{\omega_2} \int_{{\omega_1}_{LO}}^{{\omega_1}_{HI}} \frac{d\omega_1}{\omega_1} \int_{b_l o}^{{b_h}^i} \frac{db}{b}\, b^{\frac{N-m}{2}} \int_{\phi=0}^{\phi=2\pi} d\phi\ \exp(-\frac{b}{2}\sum_{j=1}^{m} {\chi^2}_{Wj}) \\ &\times \prod_{j=1}^{m} \{{W_j}^{-1/2}\,[\text{erfc}(y_{jmin}) - \text{erfc}(y_{jmax})\ ]\}, \end{aligned} \tag{48}$$

where $\omega_2 = \frac{2\pi}{P_2}$ and $C =$ is a normalization constant, equal to the integral of the right hand side of above equation over ω_2.

$$\begin{aligned} p(\omega_2 \mid D, H_4, I) &= \sum_{m=2}^{m_{\max}} p(M_m, \omega_2 \mid m > 1, D, I) \\ &= \sum_{m=2}^{m_{\max}} p(M_m \mid D, I)\ p(\omega_2 \mid D, M_m, I), \end{aligned} \tag{49}$$

where

$$p(M_m \mid D, I) = \frac{p(M_m \mid I)\ p(D \mid M_m, I)}{\sum_{m=2}^{mmax} p(M_m \mid I)\ p(D \mid M_m, I)} = \frac{p(D \mid M_m, I)}{\sum_{m=2}^{mmax} p(D \mid M_m, I)} \tag{50}$$

and $p(\omega_2 \mid D, M_m, I)$ from equation (48). Equation (49) is a weighted sum of the marginal posteriors for all the periodic models being considered, from those with $m = 2$ to $m = m_{\max} = 12$.

The posterior probability of P_1 is given by equation (49) replacing ω_2 by ω_1 and with $p(\omega_1 \mid D, M_m, I)$ given by,

$$p(\omega_1 \mid D, M_m, I) = \frac{C}{\omega_1} \int_{{\omega_1}_{LO}}^{{\omega_1}_{HI}} \frac{d\omega_2}{\omega_2} \int_{b_l o}^{b_h i} \frac{db}{b}\ b^{\frac{N-m}{2}} \int_{\phi=0}^{\phi=2\pi} d\phi\ \exp(-\frac{b}{2}\sum_{j=1}^{m} {\chi^2}_{Wj}) \times \prod_{j=1}^{m} \{{W_j}^{-1/2}\,[\mathrm{erfc}(y_{jmin}) - \mathrm{erfc}(y_{jmax})\ ]\}, \tag{51}$$

6.3. Estimating the Shape of the Timing Residual Modulation.

The mean light curve shape for a given M_m, after marginalizing over all the other parameters follows directly from equations 55 and 50 of Paper I. It is only necessary to marginalize over the additional period or ω_1. The mean $r(t)$ is then given by,

$$\langle r(t) \mid m\rangle = \int d\omega_1 \int d\omega_2 \int db \int d\phi\ \overline{\tau_{Wj}}\ p(\omega_1, \omega_2, b, \phi \mid D, M_m, I), \tag{52}$$

where $p(\omega_1, \omega_2, b, \phi \mid D, M_m, I)$ is given by

$$p(\omega_1, \omega_2, b, \phi \mid D, M_m, I) = \frac{(\omega_2 b)^{-1} \prod_{j=1}^{m} \{(bW_j)^{-1} F \exp(-\frac{b}{2}\sum_{j=1}^{m} \chi^2_{Wj})\}}{\int \frac{d\omega_1}{\omega_1} \int \frac{d\omega_2}{\omega_2} \int \frac{db}{b} \int d\phi \prod_{j=1}^{m} \{(bW_j)^{-1} F \exp(-\frac{b}{2}\sum_{j=1}^{m} \chi^2_{Wj})\}}, \tag{53}$$

and,

$$F = \left[\mathrm{erfc}(\frac{bW_j}{2}(r_{min} - \overline{\tau_{Wj}})) - \mathrm{erfc}(\frac{bW_j}{2}(r_{max} - \overline{\tau_{Wj}}))\right]. \tag{54}$$

Finally we marginalize over m to obtain,

$$\langle r(t) \mid H_4\rangle = \langle r(t) \mid m > 1\rangle = \sum_{m=2}^{m_{\max}} p(M_m \mid D, I)\ \langle r(t) \mid m\rangle, \tag{55}$$

The calculation of the mean standard deviation of the estimate of $r(t)$ proceeds analogously. We simply replace $\overline{\tau_{Wj}}$ by $\sqrt{(bW_j)^{-1}}$ in equation (52).

7. Results for H_4 and Comparison of the four Hypotheses

The most probable periods, noise scale parameters, b, and timing residuals for the four models are given in Table 1. It is clear that H_4 has a significantly smaller timing residual than the other three models but it also has more parameters.

To determine whether the greater complexity of H_4 is justified we need to compute the Bayesian odds ratio which is the ratio of the probability of H_4 to each of the other three models. The ratio, $O_{41} = p(H_4 \mid D, I)/p(H_1 \mid D, I)$, is called the *odds ratio* in favor of model H_4 over model H_1. Application of Bayes's theorem leads to,

$$O_{41} = \frac{p(H_4 \mid I)}{p(H_1 \mid I)} \frac{p(D \mid H_4, I)}{p(D \mid H_1, I)} \equiv \frac{p(H_4 \mid I)}{p(H_1 \mid I)} B_{41} \tag{56}$$

where the first factor is the prior odds ratio, and the second factor is called the *Bayes factor*. The Bayes factor is the ratio of the global likelihoods of the models. As discussed in detail in GL2, the Bayes factor automatically includes a quantitative Occam's razor penalizing (through the global likelihoods) H_4 for its extra complexity.

The computed Bayes factors are $B_{41} = 1.4 \times 10^{11}$, $B_{42} = 2,710$ and $B_{43} = 1.4 \times 10^{9}$. Assuming equal prior probabilities for the four hypotheses, H_4 is found to be much more probable than the other three models. In addition, the gravitational energy release associated with an $\approx 1\%$ sudden change in period required for H_2 would be comparable to supernova energies making this model very unlikely due to an absence of any dramatic change in its other properties and no report of a Galactic supernova. We can therefore safely claim to have demonstrated a periodic modulation to the outburst timing residuals and now proceed to examine this in more detail.

Figure 5(a) shows the marginal posterior probability of the modulation period, P_2, obtained from equation (49) for the same period range as shown in Figure 2(b) of Paper I. The mean period is 1580 days with a 68% credible region from 1571 to 1589 days.

The marginal posterior probability for the outburst period, P_1, shown in figure 5(b), is given by equations (49), with the terms involving ω_1 and ω_2 interchanged, together with equation (51).

Figure 6(a) shows the shape estimate for the outburst timing residual modulation plotted for two cycles of P_2 phase, derived from equation (55). The solid curves show ± 1 standard deviation estimates. The phase was computed using a modulation period $P_2 = 1580$ days and set $= 0$ at Julian Day 2,443,366.775 by convention. The individual outburst timing residuals, computed on the basis of the most probable value of the outburst period, $P_1 = 26.491$ days, and are over plotted together with their error bars.

The agreement is remarkably good, although around phase 0.35 the estimated shape sigma is larger due to a paucity of data in this region. Note that the shape estimate is essentially a weighted superposition of stepwise light curves with different numbers of bins, each with different phase, noise scale factor and periods P_1 and P_2, with weights given by the probability densities for

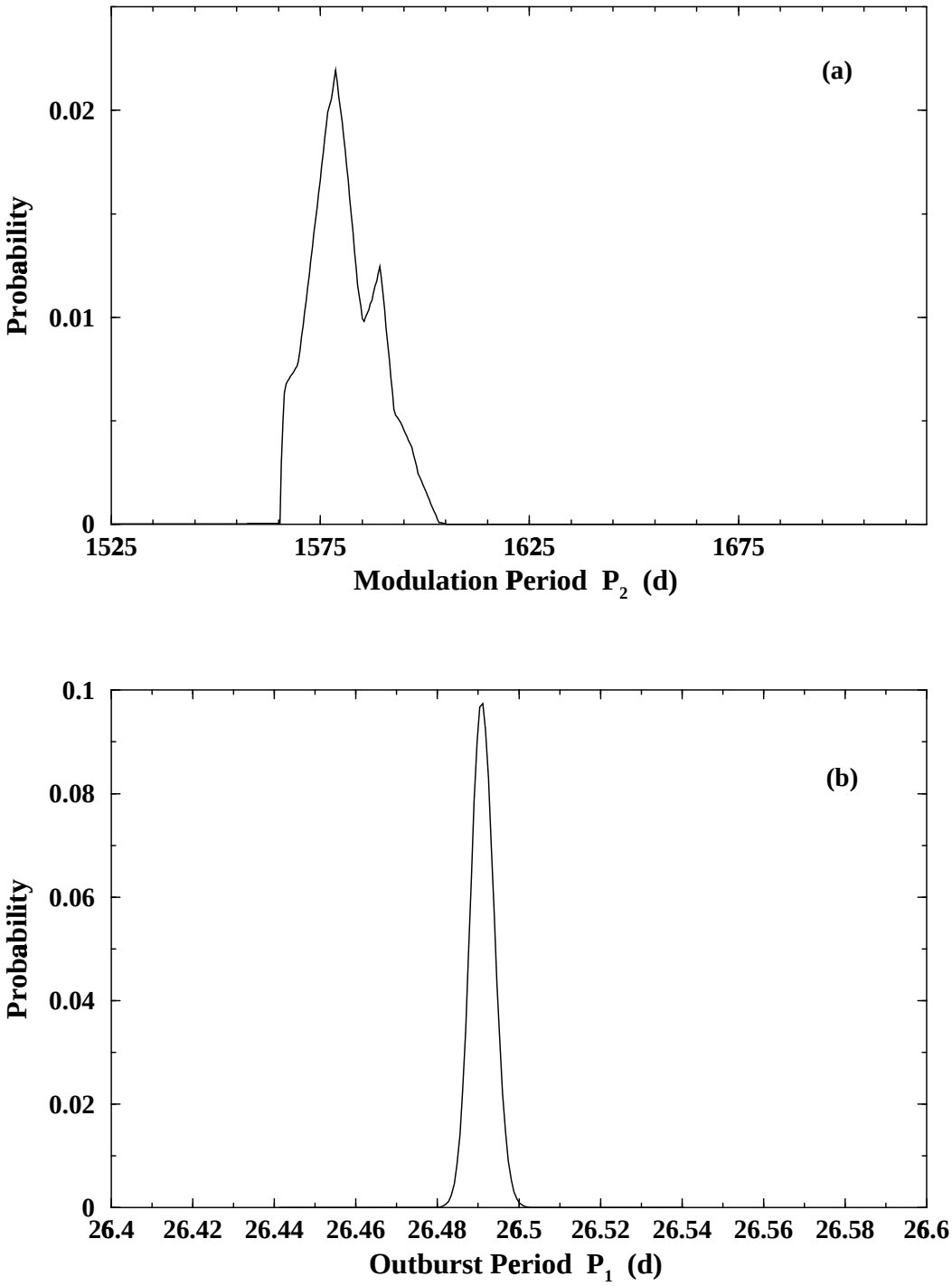

Fig. 5.— The marginal probability densities of (a) the modulation period for the timing residuals of the LS I +61°303 outbursts and (b) the outburst period, P_1.

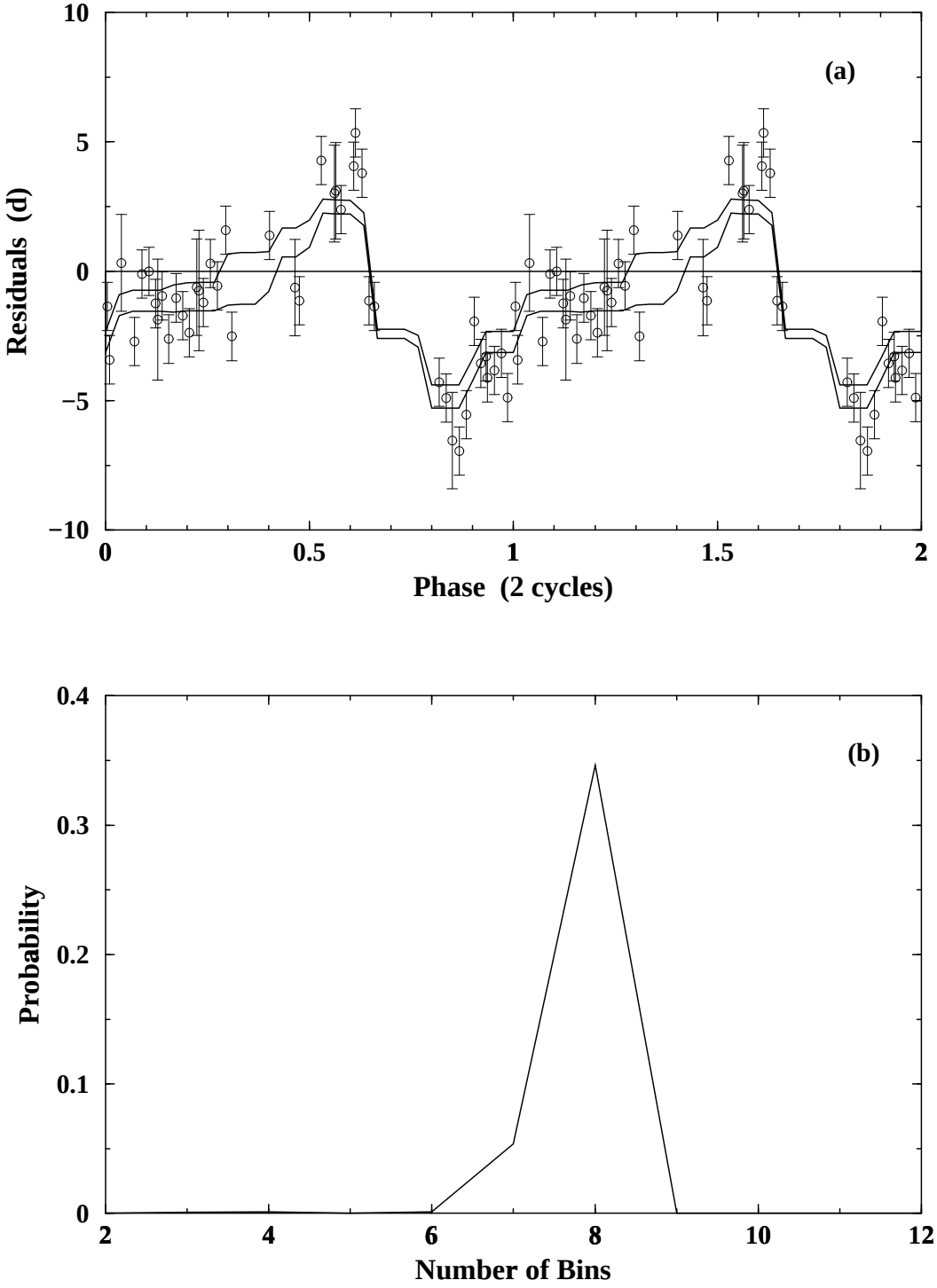

Fig. 6.— In (a) the two solid curves are the estimated mean light curve, ±1 standard deviation, of the periodic modulation ($P_2 = 1580$ days) of the LS I +61°303 outburst timing residuals for two cycles of phase. The individual timing residuals computed for the most probable outburst period ($P_1 = 26.491$ days) are also shown. The lower panel (b) shows the marginal posterior probability of the number of bins for model H_4.

these parameters. It is thus not a stepwise function, but rather a somewhat smoothed version of a stepwise function. The underlying shape suggested by this result is a roughly sawtooth pattern with a gradual rise and rapid fall.

Figure 6(b) shows the marginal posterior probability of the number of bins, m. For the present state of information the maximum occurs for $m = 6$. We anticipate that as further data is acquired the evidence will overcome the higher Occam penalty associated with larger values of m, resulting in a further shift to the right and a more accurate delineation of the modulation.

8. Joint Analysis of Outburst Phase and Flux Modulations

Paper I provided convincing evidence for a long term modulation of the peak outburst flux with a mean period of 1632 days and a 68% credible region of 1599 to 1660 days. In this paper we have found convincing evidence for a long term modulation of the outburst timing residuals. The two modulation period probability distributions overlap just outside their 68% credible regions. It therefore appears very likely that these two phenomena are related and more than likely that they have the same period.

We now introduce a fifth hypothesis $H_5 \equiv$ "Both timing residuals and flux are periodically modulated with the same period". We let $D_F \equiv \{S(t_i)\}$, the set of outburst peak flux densities for outbursts occurring at a set of times $\{t_i\}$. It is not necessary that this set of outbursts be exactly the same as the set of outburst defined by D in equation (2), because the accuracy required to be useful in inferring a value of the long term modulation period, P_2, from flux modulation data is less than that required for estimating P_2 from the timing residuals associated with a much shorter outburst period.

We can readily compute the most probable value of a common modulation period and explore the possible relationship between outburst flux and timing modulation in orbital phase. The posterior probability of P_2, the period of the outburst timing residual modulation, follows from a simple modification of equations 38 and 39 of Paper I.

$$\begin{aligned} p(\omega_2 \mid D, D_F, M_m, I) &= p(\omega_2 \mid D_F, I)\, \frac{p(D \mid \omega_2, D_F, M_m, I)}{p(D \mid D_F, M_m, I)} \\ &= p(\omega_2 \mid D_F, I)\, \frac{p(D \mid \omega_2, M_m, I)}{p(D \mid M_m, I)} \end{aligned} \tag{57}$$

where $p(\omega_2 \mid D_F, I) =$ the posterior probability density function for ω_2 obtained from an analysis of D_F in Paper I. Thus $p(\omega_2 \mid D_F, I)$ replaces the earlier Jeffreys prior for ω_2 in equation 10 of Paper I. In these equations M_m stands for the m bin periodic model used to describe the shape of the timing residual modulation and not the flux modulation. In equation (57), $p(D \mid M_m, I)$, merely plays the role of a normalization constant. The result is,

$$p(\omega_2 \mid D, D_F, M_m, I) = C\, p(\omega_2 \mid D_F, I) \int_{\omega_1{}_{LO}}^{\omega_1{}_{HI}} d\omega_1 \int_{b_{LO}}^{b_{HI}} \frac{db}{b}\, b^{\frac{N-m}{2}} \int_{\phi=0}^{\phi=2\pi} d\phi\ \exp(-\frac{b}{2}\sum_{j=1}^{m} {\chi^2}_{Wj}) \times \prod_{j=1}^{m} \{{W_j}^{-1/2}\,[erfc(y_{jmin}) - erfc(y_{jmax})\ ]\}, \quad (58)$$

where $C =$ is a normalization constant, equal to the integral of the right hand side of above equation over ω_2 and the other terms are the same as in section 6.1. The remainder of the calculation follows from section 6.2

$$\begin{aligned} p(\omega_2 \mid D, D_F, H_5, I) &= \sum_{m=2}^{m_{\max}} p(M_m, \omega_2 \mid m > 1, D, D_F, I) \\ &= \sum_{m=2}^{m_{\max}} p(M_m \mid D, D_F, I)\ p(\omega_2 \mid D, D_F, M_m, I) \\ &= \sum_{m=2}^{m_{\max}} p(M_m \mid D, I)\ p(\omega_2 \mid D, D_F, M_m, I), \end{aligned} \quad (59)$$

where

$$\begin{aligned} p(M_m \mid D, I) &= \frac{p(M_m \mid I)\ p(D \mid M_m, I)}{\sum_{m=2}^{mmax} p(M_m \mid I)\ p(D \mid M_m, I)} \\ &= \frac{p(D \mid M_m, I)}{\sum_{m=2}^{mmax} p(D \mid M_m, I)} \end{aligned} \quad (60)$$

and $p(\omega_2 \mid D, D_F, M_m, I)$ is from equation (58). Equation (59) is a weighted sum of the marginal posteriors for all the periodic models being considered, from those with $m = 2$ to $m = m_{\max} = 12$.

Figure 7(a) shows the marginal posterior probability of the outburst timing residual modulation period, obtained from equation (59). The location of the maximum is unchanged but the probability density has increased toward larger values of P_2 than before with a new mean of 1584 days. The new 68% credible is from 1573 to 1598 days. There was no significant change in the posterior probability o P_1 and so this was not replotted. The mean P_1 only changed from 26.4911 to 26.4917 days. The 68% credible error for P_1 is ± 0.0025 days.

In a similar way the equations, given in section 6.3, for the mean shape and standard deviation of the timing residuals modulation were modified to make use of the prior $p(\omega_2 \mid D_F, I)$. This did not result in a significant change to the mean timing residual light curve and is not replotted. In addition the mean shape of the peak outburst flux modulation (Paper I) was recomputed marginalizing over the resultant P_2 probability density function given in figure 7(a). This was to enable a detailed comparison to be made between the flux and timing residual modulations to provide insight into the underlying mechanism giving rise to the modulation. Figure 7(b) shows

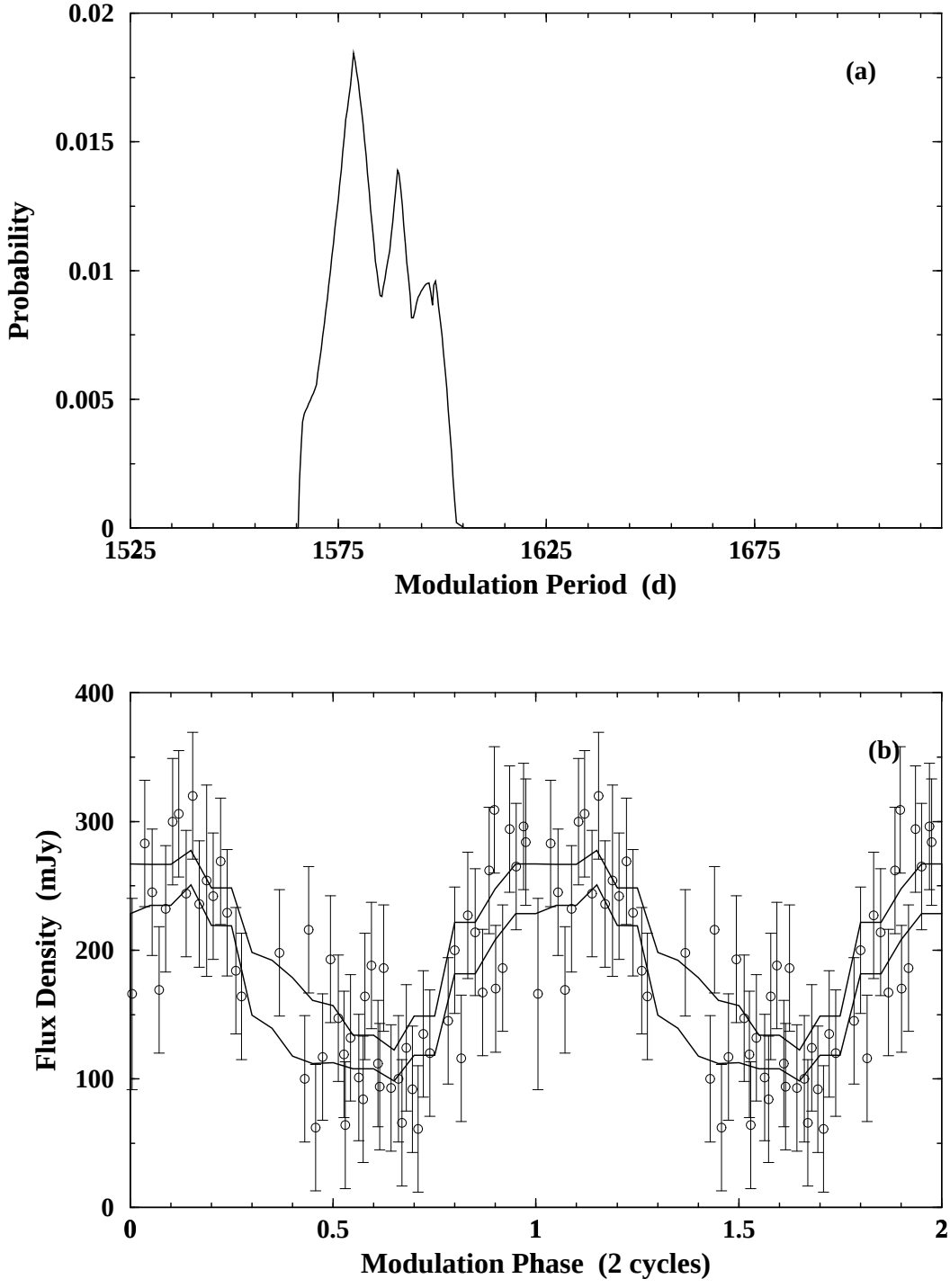

Fig. 7.— Panel (a) shows the marginal probability density of the modulation period for the timing residuals assuming a prior based on the flux modulation analysis of Paper I. Panel (b) shows the shape estimate for the outburst peak flux modulation compared to the data for two cycles of phase. The solid curve is the Bayesian estimated mean shape ±1 standard deviation.

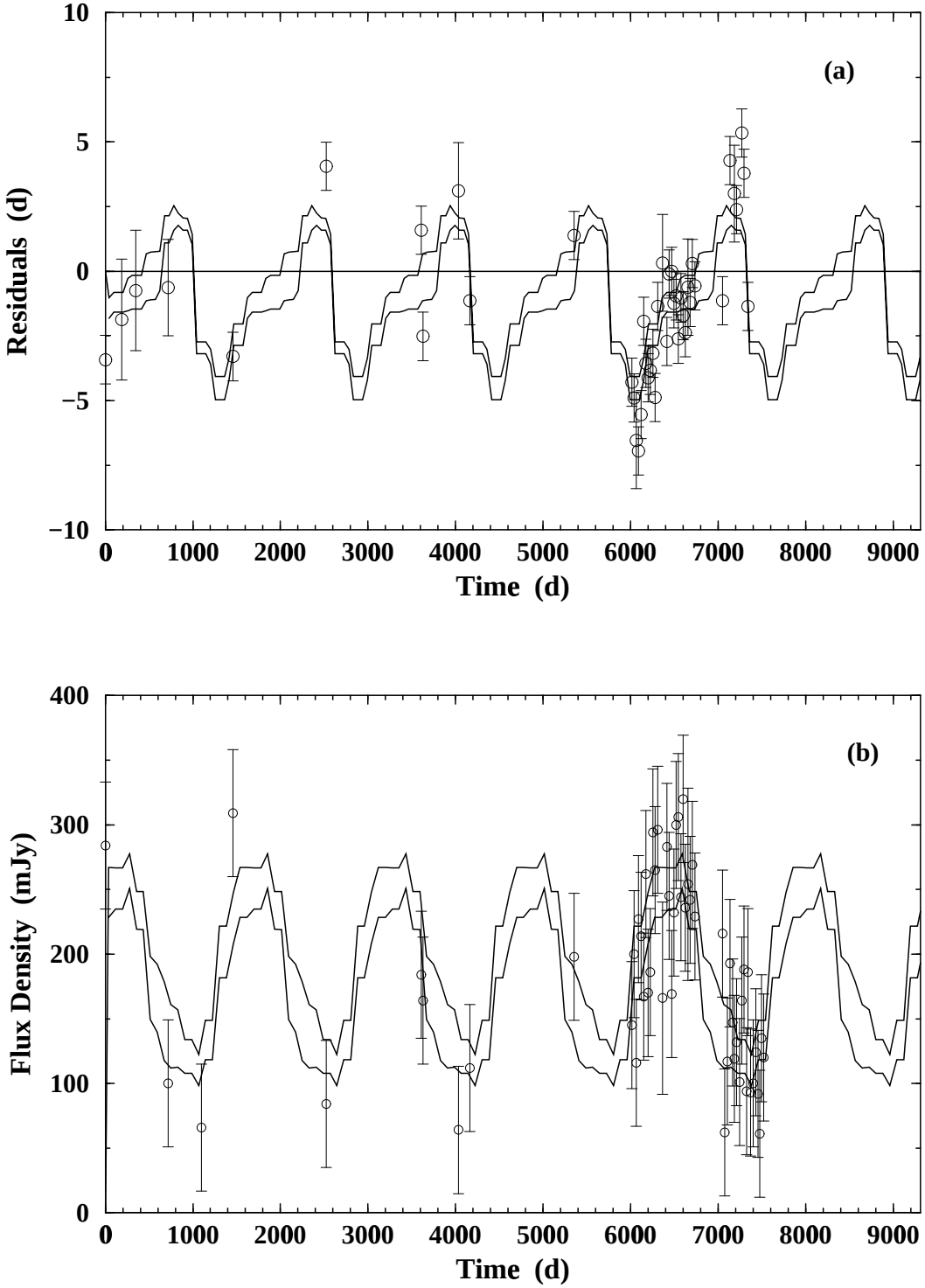

Fig. 8.— The upper panel (a) compares the predicted outburst timing residual modulation with the data versus time. The solid curves show the mean timing residual ±1 one standard deviation, while (b) compares the predicted outburst peak flux modulation with the data versus time.

this resulting flux modulation light curve for two cycles of phase. For both figures the phase was set = 0 at Julian Day 2,443,366.775 by convention.

Figures 8(a) and (b) show the predicted outburst timing residuals and peak flux ±1 standard deviation versus time compared to the data. In these plots the zero point of the time axis corresponds to Julian Date 2,443,366.775 by convention. Figure 8(a) indicates that we are about to see a rapid increase in the peak flux with the next maximum occurring between Julian Day 2,451,233 and 2,451,633.

9. Discussion

We have succeeded in demonstrating that both the outburst timing residuals and peak flux density exhibit a periodic modulation on the same time scale. The mean value of timing residual or phase modulation period, P_2, is 1584 days with a 68% confidence interval of 1573 to 1598 days. The timing residuals reach a maximum of $\approx +5$ days around P_2 phase of 0.6 and a minimum of ≈ -6 days at P_2 phase of 0.85. The flux on the other hand is a minimum in the range 0.6 to 0.7, climbing thereafter to reach a broad maximum in the range of P_2 phase between 0.95 to 0.25 .

It is of great interest to relate the current results to previous observations at other wavelengths within the framework of an overall model for the system. We will use as our starting point the supercritical accretion model (Taylor and Gregory 1982, Taylor et al. 1992, Martí and Paredes 1995) and suggest the needed modifications towards the end of this section. We will also use the orbital model proposed by Martí and Paredes (1995) based on near infrared observations. Their analysis suggests an eccentric orbit (e $\approx$ 0.7) with periastron passage at radio outburst phase of 0.53 and apastron at 0.03. The radio phase is computed from the orbital period with radio phase set = 0 at Julian Day 2,443,366.775 by convention. The timing residuals in this analysis are based on our most probable orbital period of 26.491 days and are measured with respect to outburst 28 (Julian Day 2,449,850.01) which corresponds to a radio phase of 0.74. Thus the timing residuals range from -6 to +5 days corresponds to a radio phase range from $\approx$ 0.52 to 0.93 or from around periastron to close to apastron.

Taylor et al. (1992) computed the accretion rate on to a neutron star secondary in orbit within the equatorial wind of the Be star primary for a variety of eccentricities. For $e > 0.4$ two accretion peaks occur. The biggest corresponds to periastron passage through the densest portion of the wind and a second smaller peak occurs at a later phase when the relative velocity of receding neutron star and the Be star wind is a minimum. Martí and Paredes (1995) investigated the variation of this structure with Be star wind velocity and found that both the height and delay of the second peak is a function of the Be star wind velocity. A variation of wind velocity from 20 to 2 km/s results in a variation in the radio phase of the peak from 0.62 to 0.92 for $e = 0.7$. Also the secondary peak is higher and narrower the larger the wind velocity. For accretion on to a naked neutron star the accretion rate becomes supercritical for a narrow range of phase about

both peaks and this situation is very likely to give rise to the acceleration of relativistic electrons through the production of shock waves.

Since the wind is opaque at radio wavelengths the relativistic electrons must propagate out of the orbital plane to give rise to radio outburst. Relativistic electrons produced near periastron will suffer severe inverse Compton losses, due to proximity to the Be primary (Martí and Paredes 1995) and lose their energy before they can propagate out of the opaque wind to produce a radio outburst. Thus we expect an X-ray and possible gamma-ray outburst but no radio outburst. Simultaneous X-ray and radio observations for one orbital cycle (Taylor et al. 1996) found an X-ray outburst at radio phase 0.5 (periastron) and a delayed radio outburst around phase 0.95 (Julian Day 2,448,850.07). For the second accretion peak the neutron star is much further from the primary and inverse Compton losses will be much less and the wind less opaque at radio wavelengths.

The main problem with the above model is that the peak X-ray luminosity of LS I +61°303 of $\approx 10^{34}$ erg s^{-1} (Taylor et al. 1996) is much less then the $\geq 10^{38}$ erg s^{-1} expected for accretion to the surface of a neutron star but still much greater than that expected for a white dwarf secondary at a distance $\approx$ 2 kpc (Frail and Hjellming 1991). If the COS B and GRO γ-ray emission is associated with LS I +61°303, then luminosities of 10^{36} - 10^{37} erg s^{-1} are inferred. Campana et al. (1995) have suggested that the accreting matter is stopped at the magnetospheric radius by the centrifugal barrier produced by a magnetosphere rotating at a super-Keplerian rate resulting in a much lower accretion luminosity of order 10^{35} erg s^{-1}. In any case there will still be two peaks in the accretion rate one associated with periastron and the another when the neutron star is moving towards apastron and its relative velocity to the wind is minimum. Modulation in the wind velocity could then give rise to variations in the size and location of this second peak which is associated with the radio emission for the reasons described above.

Our analysis of the timing residuals suggest that the location of the secondary accretion peak can vary from close to periaston to close to apastron and that outbursts have a maximum flux when the secondary peak is around P_2 phase 0.95 to 0.28 or radio phase 0.6 to 0.7 . If we assumed accretion to a fixed magnetosphere radius then the calculations of Martí and Paredes (1995) would suggest variations in the Be star wind speed ranging from < 2 km s^{-1} to > 20 km s^{-1} at the surface of the star. This velocity range is typical of the high density equatorial disc wind region according to a study of the UV line profiles and IR excess of 10 Be stars carried out by Lamers and Waters (1987). The UV line emission is formed in the high velocity low density polar region and the IR excess is mainly due to th disc region. The exact radius at which the magnetosphere stops the accreting matter will be a function of accretion rate. Now that we have the timing residual and flux modulation light curves it is worth carrying out more detailed calculations to compare with these. We might even be able to distinguish transitions between the different accretion regimes (e.g. Lipunov 1992; Zamanov 1995).

In the context of the variable Be wind model, the shape of timing residual modulation

indicates a rapid transition from a low velocity wind of a high wind velocity occurring between P_2 phase 0.6 and 0.85. This suggests a rather sudden onset to each new cycle of mass loss by the Be star.

Finally we note that within many of the 26.5 day radio outbursts there is evidence for considerable modulation of the radio emission (referred to in Paper I as shorter duration flaring). The neutron star is always in motion relative to the Be star wind and thus the modulation of the radio emission within individual outbursts may reflect a modulation in the wind density and or velocity on relatively short distance scales. This possibly indicates some form of streaming motion or shell structure within the equatorial wind. If the Be star's equatorial mass loss rate was dependent on longitude then this would give rise to a spiral steaming motion in the wind. A more detailed analysis of the radio structure might yield a map of the wind geometry.

10. Conclusions

In this paper we considered four hypotheses to explain the outburst phase variations. From an analysis of over 20 years of radio measurements of LS I +61°303 we conclude that the phase of the periodic radio outbursts varies periodically with the same period as the outburst peak flux modulation. Combining the outburst phase and flux data we derive a phase and flux modulation period of 1584^{+14}_{-11} days as well as a more accurate outburst period of 26.4917 ± .0025 days. From the shape of the outburst timing residual modulation (outburst phase modulation) and flux modulation we find that larger outbursts occur at an earlier orbital phase, closer to periastron, probably as a result of variations in the wind from the rapidly rotating Be star primary. The phase modulation also suggests a rather sudden onset to each new cycle of mass loss by the Be star. The outburst phase and flux modulation light curves derived here provide scope for more detailed modeling of the interactions between the Be star wind and the orbiting neutron star.

Our analysis predicts that next maximum in the outburst peak flux modulation will occur between Julian Day 2,451,233 to 2,451,633. Continuation of the GBI monitoring program of LS I +61°303 for another 2 years would permit the predictions of this work to be tested and provide the needed regular high quality measurements required to disentangle the next level of source properties which are beginning to emerge.

The authors wish to acknowledge Elizabeth Waltman for her helpful comments on a first draft of the paper. During 1994-1996.3 the Green Bank Interferometer was operated by the NRAO for the Naval Research Laboratory; and during the time period 1996.8-1998 the instrument was operated by the NRAO in support of the NASA high energy program. The NRAO is operated by Associated Universities, Inc., under contract with the National Science Foundation. This research was supported in part by grants from the Canadian Natural Sciences and Engineering Research Council at the University of British Columbia and the University of Calgary.

REFERENCES

Bignami, G. F., Caraveo, P. A., Lamb, R. C., Market, T. H., and Paul, J. A. 1981, ApJ, 47, L85

Campana, S., Stella, L., Mereghetti, S., and Colpi, M. 1995, A&A, 297, 385

Frail, D. A. and Hjellming, R. M. 1991,AJ, 101, 2126

Goldoni, P., and Mereghetti, S. 1995, A& A, 299, 751

Gregory, P. C. and Taylor, A. R. 1978, Nature, 272, 704

Gregory, P. C., Xu, Huang-Jian, Backhouse, C. J., Reid, A. 1989, ApJ, 339, 1054

Gregory, P. C., and Loredo, T. J. 1992a, in Maximum Entropy and Bayesian Methods, ed. C. R. Smith, G. J. Erickson, and P. O. Neudorfer (Kluwer, Dordrecht), 79

Gregory, P. C., and Loredo, T. J. 1992b, ApJ, 398, 146

Gregory, P. C., and Loredo, T. J. 1993, in Maximum Entropy and Bayesian Methods, Paris, 1992, ed. Mohammad-Djafari and G. Demoment (Kluwer, Dordrecht), 225

Gregory, P. C., and Loredo, T. J. 1996, ApJ, 473, 1059

Gregory, P. C. 1999, ApJ(in press)

Kniffen, D. A. et al. 1997, ApJ, 486, 126

Lamers, H. J. G. L. M. and Waters, L. B. F. M. 1987, ApJ, 182, 80

Leahy, D. A., Harrison, F. A., & Yoshida, A. 1997, ApJ, 475, 823

Lipunov, V. M.,"Astrophysics of Neutron Stars", Springer Verlag, NY, 1992

Martí, J. 1993, PhD Thesis, Universitat de Barcelona

Martí, J. and Paredes, J. M. 1995, A&A, 298, 151

Peracaula, M. 1997, PhD Thesis, Universitat de Barcelona

Paredes, J. M., Estalella, R., Ruis, A. 1990, A&A, 232, 337

Paredes, J. M., Estalella, R., Ruis, A. 1990, A&A, 232, 337

Paredes, J.M., Martí, J., Peracaula, M. & Ribo, M. 1997, A&A, 320, L25

Ray, P. S., Foster, R.S., Waltman, E. B. et al. 1997, ApJ, 491, 381

Taylor, A. R. and Gregory, P. C. 1982, ApJ, 255, 210

Taylor, A. R. and Gregory, P. C. 1984, ApJ, 283, 273

Taylor, A. R., Kenny, H. T., Spencer, R. E. and Tzioumis, A. 1992, ApJ, 395, 268

Taylor, A. R., Young, G., Peracaula, M., Kenny, H. T., and Gregory, P. C. 1996, A&A, 305, 817

Zamanov, R. K. 1995, MNRAS,272, 308

Table 1. Periods, b values and RMS residuals.

Model	Periods (days)	b Value	RMS Residuals (days)
H_1	$P = 26.494^{+.005}_{-.006}$ d	0.18	2.8
H_2	$P_1 = 26.509 \pm .011$ d	0.24	2.3
	$P_2 = 26.649^{+.012}_{-.017}$ d	0.55	1.6
H_3	$P = 26.618^{+.010}_{-.011}$ d	0.25	2.4
	$\dot{P} = 1.04^{+.05}_{-.06} \times 10^{-4}$ d/d		
H_4	$P_1 = 26.491 \pm .0025$ d	1.13	1.4
	$P_2 = 1580 \pm 9$ d		